

# 2-Carbamido-1,3-indandione – a Fluorescent Molecular Probe and Sunscreen Candidate

Venelin Enchev<sup>1</sup> · Ivan Angelov<sup>1</sup> · Vanya Mantareva<sup>1</sup> · Nadezhda Markova<sup>1</sup>

Received: 17 April 2015 / Accepted: 18 August 2015  
© Springer Science+Business Media New York 2015

**Abstract** The present work reports theoretical and experimental studies on the photophysical properties of two tautomeric forms of 2-carbamido-1,3-indandione (CAID). By means of UV-vis, steady-state and time-dependent fluorescence spectroscopy it is shown that both enol forms, 2-(hydroxylaminomethylidene)-indan-1,3-dione and 2-carboamide-1-hydroxy-3-oxo-indan, coexist in solution. On the base of spectroscopic studies of CAID interaction with human serum albumin and DNA sequences, it was shown that the compound has potential and it is suitable for use as fluorescent molecular probe for investigation of different biomolecules. CAID shows relatively high photostability within 3 h irradiation period. Such behavior of the investigated compound supposes possibilities for using of the CAID molecule as sunscreen because of strong absorption in UVA, UVB and UVC light spectra.

**Keywords** 2-carbamido-1,3-indandione · Tautomerism · Fluorescence · Sunscreen

## Introduction

The syntheses of 2-carbamido-1,3-indandione (CAID) was reported by Horton and Murdock [1] but for a long time its structure was not elucidated. The compound exists in the solid state as yellow–orange needles, which sinter from 180 to 220 °C [1]. On the basis of ab initio quantum-

chemical calculations and NMR, IR and UV-vis spectroscopy Enchev et al. [2, 3] showed that two enol tautomeric forms, 2-(hydroxyl-aminomethylidene)-indan-1,3-dione (A) and 2-carboamide-1-hydroxy-3-oxo-indan (B), coexist in solution (Fig. 1).

Later both enol tautomers, on amide carbonyl (A) and on ring carbonyl (B), of *N-p*-methoxyphenyl-2-carbamido-1,3-indandione were isolated and their X-ray structures determined by Rappoport et al. [4]. X-ray diffraction of the *N-o*, *p*-dimethoxy analogue indicated a disorder ascribed to the presence of a 6:4 mixture of A and B. B3LYP/6-31+G\* calculations gave good agreement with observed geometries and the calculated energies indicated that enol A is more stable by less than 1 kcal mol<sup>-1</sup> than enol B [4].

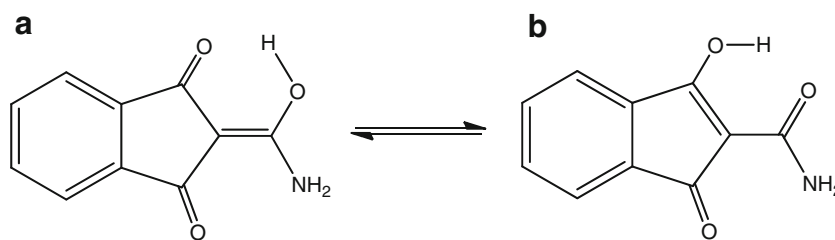
In the last decade considerable scientific interest has focused on the development of new fluorescent probes. This is motivated by the high sensitivity and selectivity of different fluorescent methods implicated in the investigation of processes at microlevel in biological objects [5].

Generally, in cells and tissues fluorescent probes are distributed randomly and inhomogeneously. Therefore, the intensity of the observed fluorescence signal is dependent not only on the local concentration of the sensors but also on illumination intensity, surroundings, optical path length, bleaching and other processes. In order to minimize the effects of these factors, fluorescent sensors that exhibit a significant spectral shift upon reaction or binding to the investigated object are preferred for use. It is well known that analyzing concentrations of biological macromolecules with the help of fluorescent sensors, more precise results are obtained if the ratio between two emission intensities at different wavelengths can be used to evaluate the investigated concentration [6]. In this respect, of particular interest are fluorescent probes exhibiting two or more well separated emission bands in organic solvents. The main advantage consists in that they are able to provide a

✉ Venelin Enchev  
venelin@orgchm.bas.bg

<sup>1</sup> Institute of Organic Chemistry, Bulgarian Academy of Sciences, 1113 Sofia, Bulgaria

**Fig. 1** Equilibrium between tautomeric forms 2-(hydroxyaminomethylidene)-indan-1,3-dione, (**a**), and 2-carboamide-1-hydroxy-3-oxo-indan, (**b**)



reliable ratiometric signal in different bands, which bands are independent of the probe concentration and other factors [7]. In application of fluorescent methods for analysis when the ratiometric signal comes from a single dye, the different sources of error and misinterpretation are minimal. In addition, one main requirement for fluorescent probes is the absence of photobleaching. Such characteristics of fluorescence signals are often manifested by compounds with inherent tautomerism [8].

Excited-state intramolecular proton transfer (ESIPT) is very effective for the design of probes with a dual band of fluorescent signal. ESIPT results in the formation of two tautomeric forms in the excited state of the probe [9] which have well separated emission maxima. Therefore tautomers showing ESIPT as a well-known photo induced mechanism to obtaining dual fluorescent probes are real candidates for such applications. ESIPT and other dual fluorescent molecules can be used as sensitive probes of their local environment [10], including in applications such as in situ pH sensors [11] and are proposed for the study of the interaction of ligands and drugs of different nature with serum albumins [12]. Human serum albumin (HSA) is one of the major plasma proteins in the blood that contribute significantly in physiological functions and play a major role in the efficiency of drug delivery processes. For this reason, the investigation of the binding properties of CAID as a sensitive fluorescent probe to HSA is of interest.

On the other hand, for significant increasing of the sensitivity of fluorescence methods, probes should possess the potential to bind to characteristic parts of the target object. Such molecules should be able to behave as hydrogen-bond donors. This is necessary for provoking the formation of a stable complex in solution. Hydrogen bonds are directional, a feature which allows the design of receptors capable of differentiating between anions with different geometries and hydrogen-bonding requirements. Neutral receptors that contain N-H fragments can act as hydrogen-bond donors for anions, such as acetate and carboxylate anions, which are a product in many biochemical reactions [13]. A large interest exists in the development of artificial neutral receptors and fluorescent probes for anions due to their medicinal and environmental potential applications [7, 13]. DNA are other biological objects for which scientists need very sensitive fluorescent probes. Very weak intrinsic emission has been observed from

unlabeled DNA and this emission is too weak and too far in the UV which makes it unusable for practical applications. Fortunately, there are numerous probes that spontaneously bind to DNA and display enhanced emission [14]. The most widely used fluorescent probes for DNA investigations such as ethidium bromide and 4',6-diamidino-2-phenylindole have an amino group in their structure and bind spontaneously to the DNA via hydrogen bonds or proton transfer [5] and therefore CAID will be with potential capabilities to bind to the nucleobases of DNA and RNA. Interactions of small molecules with DNA have been studied for several decades because of hope for better understanding of design principles for the targeting of specific DNA sequences in order to control gene expression. We note that, the native bases of DNA are not useful as fluorescent probes, and thus the use of extrinsic DNA probes is necessary. For this reason the potential possibilities of use of CAID in investigations of DNA or in DNA sequencing is interesting.

In the last years scientists working in the sphere of human health try to inform the community of the different risks for people exposed to sun radiation. Sun radiation includes x-ray, ultraviolet, visible and infrared light, and radiowaves. UV light, which is the main part of sun radiation dangerous for people, can be subdivided into three bands according to wavelength: UVA (320–400 nm), UVB (290–320 nm) and UVC (200–290 nm). The total flux of UVA at the earth's surface vastly exceeds that of UVB, with all the UVC being completely absorbed by stratospheric ozone [15]. Depending on the latitude, the time of the day and the season of the year, the terrestrial spectrum of solar UV radiation consists of 1–5 % of UVB radiation and 95–99 % of UVA radiation. UVB radiation is fully absorbed by the stratum corneum and the top layers of the epidermis, whereas up to 50 % of incident UVA radiation penetrates Caucasian skin deep into the dermis [16].

Both UVB and UVA radiation may affect the biomolecules of the skin. UVB radiation is erythemalogenic, carcinogenic, induces photoaging and mutagenic damage to nucleic acids. UVB is directly absorbed by DNA, giving rise to dimeric photoproducts between adjacent pyrimidine bases [17]. Furthermore, UVB photoisomerizes trans- to cis-urocanic acid (a prominent candidate chromophore for mediating photoimmunosuppression) [18] and generates reactive oxygen species (ROS) [19], suggesting that UVB also employs an indirect mechanism for its detrimental effects. UVA is also

mildly erythemagenic, but promotes ROS accumulation. ROS induce direct cell damage, carcinogenesis and contribute to photoaging.

Sunscreens (UV filters) are designed to protect the skin from the harmful effects of solar radiation, particularly the UV band [15]. Visible light can also harm the skin if there is a previous skin condition, e.g. chronic actinic dermatosis, or erythropoietic porphiria. Current UV filters do not protect against visible light [20].

Sunscreens have traditionally been divided into organic (chemical) absorbers and inorganic (physical) blockers on the basis of their mechanism of action. The organic compounds absorb high-intensity UV rays with excitation to a higher energy state. Excess energy is dissipated by emission of higher wavelengths or relaxation by photochemical processes such as isomerization and tautomerisation.

In the present work we report theoretical and experimental studies of the photophysical properties of the tautomeric forms of 2-(hydroxylaminomethylidene)-indan-1,3-dione as a potential fluorescent probe and UV-protector.

## Calculations and Experimental

### Quantum-Chemical Calculations

The ground state geometries and normal mode vibrational frequencies of the equilibrium tautomeric forms and of the transition state (TS) were computed both in the gas phase and in solution at Möller-Plesset (MP2) level using different basis sets. For the optimized TS one single imaginary frequency was found in the diagonalized mass-weighted Hessian matrix, and the corresponding vibrational mode was confirmed to determine the reaction coordinate of the migration of a hydrogen atom from the hydroxyl oxygen to the carbonyl oxygen. Starting from the transition state, the reaction path was generated as the steepest descent path in mass-scaled coordinates (intrinsic reaction coordinate, IRC) using the Gonzalez-Schlegel algorithm [21], employing a step size of 0.05 Bohr (1 Bohr corresponds to 0.53 Å). On both branches of the reaction coordinate 40 steps were performed. The values of Gibbs free energies ( $\Delta G$ ) and activation barriers ( $\Delta G^\ddagger$ ) were calculated for a temperature of 298.15 K.

Solvent effect was accounted for by using the self-consistent reaction field (SCRf) method with the conductor polarizable continuum model (C-PCM) formalism [22] at MP2 level. In this model, the molecule is embedded in a cavity surrounded by an infinite dielectric which approximates the solvent as a structureless polarizable continuum characterized by its macroscopic dielectric permittivity,  $\epsilon$ . The tautomeric forms and the TS were optimized again at C-PCM/MP2/6-31+G(d) and C-PCM/MP2/6-311+G(d) levels of theory.

As it is known that the DFT methods are used as a reliable tool for the theoretical treatment of electronic structure and spectroscopic properties of various types of compounds, the stationary points on the potential energy surfaces of the ground state  $S_0$  and the first ( $\pi\pi^*$ ) singlet excited electronic state  $S_1$  of both tautomers (Fig. 1) were optimized using DFT for  $S_0$  and Time Dependent DFT (TD-DFT) [23, 24] for  $S_1$ . B3LYP functional [25, 26] and 6-31+G(d) basis set [27, 28] was chosen. Vibration frequency calculations were performed numerically for the  $S_0$  and  $S_1$  states to obtain vibrational zero point and thermal energies and to validate that the found structures corresponded to the energy minima. Bulk solvent effects on the ground and the excited states were taken into account by means of the C-PCM formalism<sup>22</sup>. The vertical excitation energies, wavelengths and associated oscillator strengths were calculated using TDDFT at the B3LYP/6-31+G(d) level at the optimized ground state geometries.

The GAMESS program [29, 30] was used to perform the ab initio, DFT and TDDFT calculations.

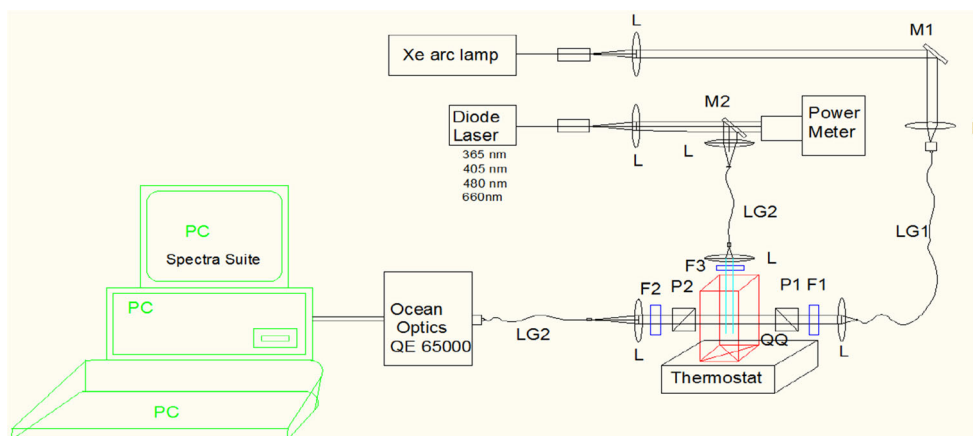
### Experimental Studies

#### Steady-State Spectral Measurements

The absorption and emission measurements were performed on a UV-Vis Jasco spectrophotometer Model VA570, fiber optics specifically elaborated spectrophotometer on the basis of Ocean Optics QE 65000 spectrophotometer with Spectra Suite Software (Scheme 1) and on Horiba Jobin Yvon Fluoreolog 3 fluorimeter, respectively.

The experimental set-up on the basis of spectrophotometer QE 65000 is shown in Scheme 1. The excitation sources for fluorescence measurements were used continuum waves (CW) Diode lasers with different wavelengths. For absorbance measurements Xe arc lamp light source and delivery components (light guide, lenses (L), several optic filters (F) and polarizers) to obtain light intensity in linear range of QE 65000 were used. Several optical fibers (LG) to deliver the excitation and registered signals in spectral range 275–800 nm were used. For fluorescence measurements the excitation power applied at the excitation wavelengths was constant of about 50 mW and the fluence rate applied in cuvette (QQ) was approximately 100 mW.cm<sup>-2</sup>. Fluorescence signals were obtained by collection fibers adjusted at a 90° position towards the excitation beam. The absorbance and fluorescence spectra were recorded using a fiber-optic micro-spectrometer QE 65000 (“Ocean Optics”, Inc., Dunedin, FL, USA). The spectral resolution of the micro-spectrometer was approximately 1 nm. The spectra were recorded using the micro-spectrometer specialized software Spectra Suite (“Ocean Optics”, Inc., Dunedin, USA). The data were analyzed and graphically represented by means of computer programme Origin 8.0 (Microcal Software, Inc., Northampton, MA, USA).

**Scheme 1** Experimental setup of fiber optics elaborated spectrophotometer on the basis of Ocean Optics QE 65000 spectrophotometer



All the collected spectra were with appropriate background correction. Only freshly prepared solutions were used for spectroscopic study and all experiments were carried out at room temperature (300 K). Fluorescence quantum yields ( $\Phi_s$ ) were determined using the following equation, where fluorescein ( $\Phi_R = 0.91$  in ethanol [31]) is used as the secondary standard.

$$\Phi_S = \Phi_R \frac{A_S}{A_R} \frac{OD_R}{OD_S} \frac{n_S^2}{n_R^2} \quad (1)$$

and  $\Phi_S$  and  $\Phi_R$  are the quantum yields,  $A_S$  and  $A_R$  are the integrated fluorescence areas,  $OD_S$  and  $OD_R$  are the absorbance values for excitation wavelength and  $n_S$  and  $n_R$  are the refractive indices of the sample (S) and reference (R) molecules, respectively.

### Time-Resolved Fluorescence Study

Fluorescence lifetimes were obtained by Time Correlated Single-Photon Counting (TCSPC) on Fluorolog-3 spectrometer (Horiba Jobin Yvon) using picosecond light pulses generated from a pico-LED source at 365 nm. The decays were deconvoluted using DAS-6 decay analysis software and the acceptability of the fits was judged by  $\chi^2$  criteria and visual inspection of the residuals of the fitted functions to the data. Time-resolved fluorescence decay (I(t)) was described by the following expression:

$$I(t) = \sum_i \alpha_i \tau_i \quad (2)$$

and the mean (average) fluorescence lifetimes were calculated using the following equation [5]:

$$\langle \tau_{i0} \rangle = \frac{\sum_i \alpha_i \tau_i^2}{\sum_i \alpha_i \tau_i} \quad (3)$$

in which  $\alpha_i$  is the pre-exponential factor corresponding to the  $i$ -th decay time constant,  $\tau_i$ .

### Photostability Study

The stock solution in a concentration of  $10^{-3}$  M 2-(hydroxyamino-methylidene)-indan-1,3-dione in ethanol was prepared. The samples for measurements were diluted in order to obtain the appropriate absorbance at the highest maximum wavelength (275 nm) to the final concentration of  $5 \times 10^{-6}$  M. The samples were irradiated by an UV medium pressure mercury lamp (400 W) available as commercial product for medical purposes (Sun, Bulgaria). The typical spectrum for light transmission of the lamp is between 250 and 450 nm. Cut off filters (VEB, Jena Glasswerk Schott & General, Jena, Germany) to remove the IR irradiation were applied. The irradiance was controlled with a radiometer (Fotron, Bulgaria) to ensure the values of  $0.14 \text{ mW.cm}^{-2}$  (280–350 nm) and  $0.41 \text{ mW cm}^{-2}$  (330–375 nm) at a distance of 35 cm. The absorption spectra were recorded for different time intervals starting from 30 min to 3 h.

### Biological and Chemical Materials

Spectroscopic grade solvents (Merck and Aldrich) were used for fluorescence and UV/Vis spectroscopy measurements. Fluorescein and Rhodamin dyes were purchased from Aldrich. HSA was purchased from Sigma. 12-mer double stranded DNA (dsDNA) sequences, purchased from Metabion, Germany were used in the experiments.

The solution of HSA were freshly prepared in 0.01 M phosphate buffered saline pH 7.2 at a concentration 0.25 mM and stored in refrigerator. A stock solution of CAID in ethanol (10 mM) was prepared and stored in dark and diluted prior the measurements. The dye-solution in microliter volume was used to obtain the desired molar ratio of the protein/CAID complexes. The final ethanol concentration in the experimental volume did not exceed 0.5 %. The preparation of the complex was carried out in thermostated (37 °C) quartz cell at constant stirring. Similar procedure also was used in preparation of DNA/CAID complexes.



## Results and Discussion

The molecular structures of the two tautomeric forms, considered for CAID, A and B, are given in Fig. 1. According to the MP2 calculations with different double and triple Pople and Dunning basis sets including polarization and diffuse functions (Table 1), enol tautomer A is more stable in the gas phase. As a whole the calculations with Pople basis sets predict smaller energy differences between tautomers A and B than Dunning ones. The energy differences between the two tautomers calculated with 6-31++G(d,p) and 6-31+G(d) basis sets or 6-311++G(d,p) and 6-311+G(d) basis sets are similar.

C-PCM optimization of both tautomers and TS is performed again at MP2/6-31+G(d) and MP2/6-311+G(d) levels. In different solvents (CCl<sub>4</sub>, CHCl<sub>3</sub>, ethanol, water) the tautomeric form A is also found to be preferred. The polarity of the solvent does not change the tautomeric equilibrium (Table 1). The activation barrier is too low and the intramolecular proton

transfer reaction is very fast. That is why both tautomeric forms coexist in solution.

The enols A and B which are stable structures in S<sub>0</sub> can be promoted to the singlet excited state through irradiation with light. Figure 2 and Table 2 show the wavelengths for the theoretically predicted maxima of absorption for A and B assuming the Franck–Condon principle (no geometry relaxation in the excited state). The calculated absorption wavelength of the S<sub>0</sub> → S<sub>1</sub> transition is calculated to appear at 373 nm and 417 nm in ethanol for tautomers A and B, respectively (Table 2). The oscillator strengths for these transitions (0.009 and 0.018 for A and B, Table 2) are not high, as expected for a π–π\* transitions. Within our theoretical procedure we have found no evidence of the presence of any low-lying excited state other than the (π,π\*) state, labeled S<sub>1</sub> for both tautomers. The S<sub>1</sub> (π,π\*) state has a HOMO–LUMO character (Table 3). The excitation of the enol structures is not localized in a particular region of the molecule as HOMO and LUMO are fully delocalized along both rings. Thus, our theoretical results disregard the role of (n,π\*) excited states in the photophysical and photochemical processes of CAID.

Analysis of the vertical excitations to higher excited states, presented in Table 2, reveals that the next allowed transition for tautomer A is S<sub>0</sub> → S<sub>4</sub> which has an oscillator strength one order of magnitude higher the transition from S<sub>0</sub> to S<sub>1</sub>. The absorption wavelength of this transition is calculated to appear at 249 nm. The oscillator strength for the S<sub>0</sub> → S<sub>5</sub> transition is quite high (0.843). The next allowed transition for tautomer B after S<sub>0</sub> → S<sub>1</sub> is the S<sub>0</sub> → S<sub>3</sub> one. The absorption wavelength of this transition is calculated to appear at 308 nm and the oscillator strength is 0.038.

For comparison with the theoretical prediction for the absorption spectra of the A and B tautomers, the UV-vis spectrum of CAID was recorded in ethanol. The obtained spectrum in the range 200–600 nm, presented on Fig. 3, shows several absorption bands in the UV region. A strong absorption band appears at 275 nm. Low intensity absorption bands can be seen at 220 nm, 302 nm and 312 nm. The most intensive band at 275 nm is accompanied by a shoulder at 250 nm. The longest wavelength peak is represented by a well-defined broad maximum at 375 nm. Experimentally obtained absorption spectra and theoretically predicted transitions are in good agreement.

After photoexcitation to the S<sub>1</sub> state, the Franck–Condon excited state is relaxed to the minimum of the first excited state S<sub>1</sub> of each of the enol forms A and B. After that the molecule may emit a photon and descent to the enol ground state S<sub>0</sub>. The energy diagram of tautomerisation of CAID and the absorption-emission processes related to the S<sub>1</sub> energy level in accordance with the theoretical investigations are shown on Fig. 4.

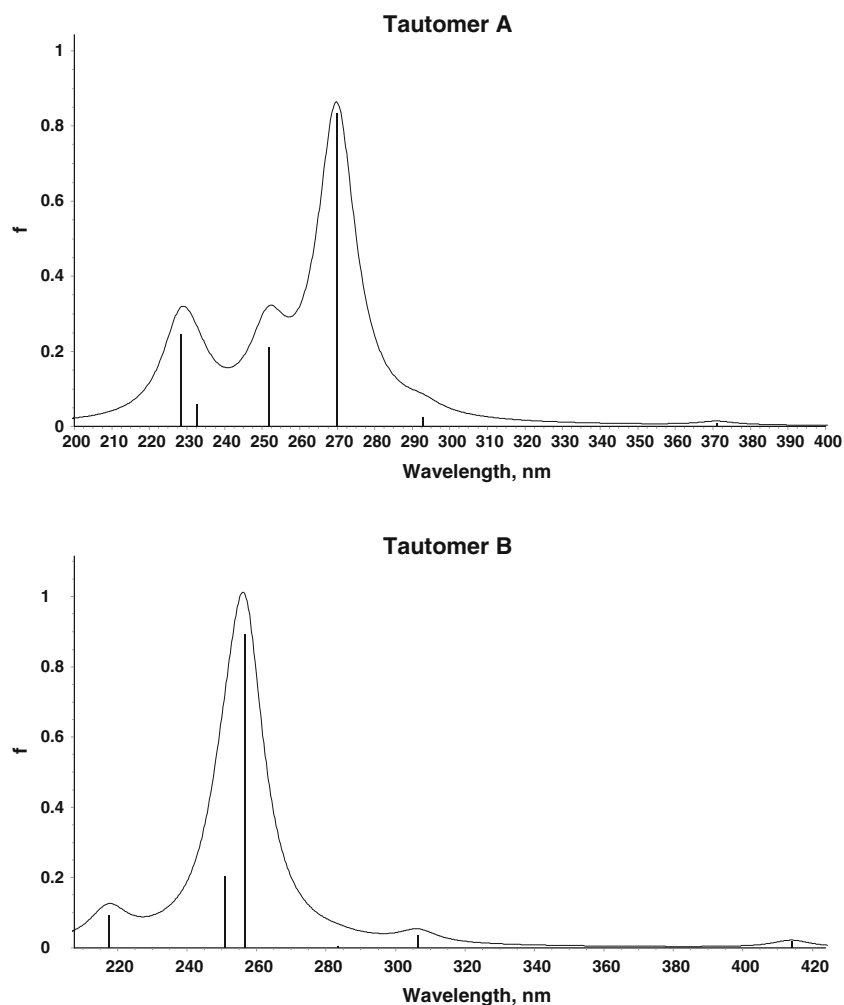
Data that can be extracted from the quantum chemical calculations are the positions of the fluorescence bands. They should correspond to the transitions from the minima of

**Table 1** MP2 calculated Gibbs free energy differences and energy barriers (kcal mol<sup>−1</sup>) for the two tautomers shown on Fig. 1, using different basis sets. Tautomer A is more stable. Imaginary frequencies are in cm<sup>−1</sup>

Computational level	$\Delta G_{298}$		$\nu^{\#}$
<b>MP2/6-31G**<sup>a</sup></b>	0.18	1.44	1161.58i
<b>MP2/6-311G**</b>	0.18	0.42	1119.01i
<b>MP2/6-31++G**</b>	0.70	1.46	1139.87i
<b>MP2/6-311++G**</b>	0.27	1.16	1123.12i
<b>MP2/6-31+G*</b>	0.57	2.41	1291.11i
<b>MP2/6-311+G*</b>	0.21	3.83	1512.38i
<b>MP2/cc-pVDZ</b>	0.86	1.04	1074.42i
<b>MP2/cc-pVTZ</b>	0.78	0.86	1057.91i
<b>MP2/aug-cc-pVDZ</b>	0.78	1.42	1164.49i
<b>MP2/aug-cc-pVTZ</b>	0.84	0.90	1090.08i
<b>MP2/6-31+G*</b>			
gas phase	0.57	2.41	1291.11i
CCl <sub>4</sub>	0.22	1.39	1261.59i
CHCl <sub>3</sub>	0.37	1.46	1257.52i
EtOH	0.26	1.23	1252.24i
water	0.59	1.46	1250.31i
<b>MP2/6-311+G*</b>			
gas phase	0.21	3.83	1512.38i
CCl <sub>4</sub>	1.41	3.10	1497.56i
CHCl <sub>3</sub>	1.52	2.58	1500.39i
EtOH	0.77	3.17	1500.48i
Water	1.03	3.35	1498.96i
<b>B3LYP/6-31+G*</b>	1.25	1.96	1192.73i
<b>B3LYP/6-311+G*</b>	1.26	2.97	1353.12i

<sup>a</sup> From Ref. [3]

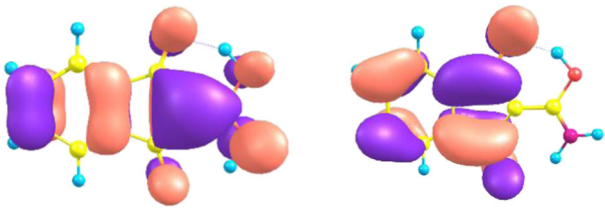
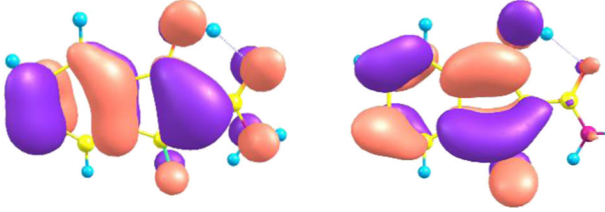
**Fig. 2** TD DFT B3LYP/6-31+G(d) calculated electronic spectra of the two tautomers of CAID in ethanol. CPCM/MP2/6-31+G(d) optimized geometry in ethanol was used



**Table 2** B3LYP/6-31+G\* calculated electronic transitions (nm) and oscillator strengths of both tautomeric forms of CAID in different solvents using MP2/6-31+G\* calculated geometries

Tautomer	Electronic transitions (oscillator strengths)					
	$S_0 \rightarrow S_1$	$S_0 \rightarrow S_2$	$S_0 \rightarrow S_3$	$S_0 \rightarrow S_4$	$S_0 \rightarrow S_5$	$S_0 \rightarrow S_6$
<b>Tautomer A</b>						
Gas	360 (0.007)	353 (0.000)	308 (0.000)	289 (0.026)	275 (0.000)	264 (0.547)
CCl <sub>4</sub>	367 (0.010)	349 (0.000)	304 (0.000)	292 (0.038)	271 (0.804)	270 (0.007)
CHCl <sub>3</sub>	370 (0.009)	347 (0.000)	302 (0.000)	293 (0.023)	271 (0.845)	267 (0.002)
EtOH	373 (0.009)	346 (0.000)	301 (0.000)	294 (0.013)	270 (0.843)	265 (0.002)
Water	373 (0.008)	345 (0.000)	301 (0.000)	294 (0.011)	269 (0.834)	265 (0.004)
<b>Tautomer B</b>						
Gas	407 (0.015)	378 (0.000)	308 (0.000)	300 (0.010)	293 (0.003)	251 (0.185)
CCl <sub>4</sub>	413 (0.021)	370 (0.000)	305 (0.031)	299 (0.000)	291 (0.004)	258 (0.883)
CHCl <sub>3</sub>	416 (0.020)	367 (0.000)	307 (0.037)	296 (0.000)	289 (0.004)	257 (0.881)
EtOH	417 (0.018)	365 (0.000)	308 (0.038)	293 (0.001)	287 (0.004)	257 (0.841)
Water	417 (0.017)	364 (0.000)	308 (0.037)	292 (0.001)	286 (0.004)	256 (0.830)

**Table 3** B3LYP/6-31+G(d) calculated transition energies ( $\lambda_{\text{calc}}$ ), oscillator strengths ( $f$ ) and frontier orbitals of tautomers **A** and **B** of 1,3-dioxo-2-indancarboxamide in ethanol

Transition	Excitation	$\lambda_{\text{calc.}}$ (nm)	$f$
<b>Tautomer A</b>			
$S_0 \rightarrow S_1$	HOMO (49) $\rightarrow$ LUMO (50) (97.3 %) HOMO LUMO	373	0.009
			
<b>Tautomer B</b>			
$S_0 \rightarrow S_1$	HOMO (49) $\rightarrow$ LUMO (50) (97.4 %) HOMO LUMO	417	0.018
			

A(B)\* down to  $S_0$  again not allowing geometry relaxation in  $S_0$ . The maxima of fluorescence in that case are predicted at 530 nm for tautomer A and 617 nm at tautomer B which values are in agreement with the experimentally measured value of 520–525 nm only for tautomer A (Fig. 5).

For obtaining the value of fluorescence quantum yield, the sample and the reference were excited at the same wavelength ( $\lambda_{\text{ex}} = 410$  nm), maintaining nearly equal absorbance (0.08) in ethanol. The determined value of fluorescence quantum yield 0.78 in saline buffer is very high and is comparable to the value 0.91 for the fluorescein, dye used as reference fluorophor.

To determine the fluorescent properties of CAID, emission-excitation spectra were investigated. The 3-D spectra are shown at Fig. 5. Intensive fluorescence in a very wide spectral range, from 330 to 600 nm, was observed. Fluorescence is off or negligible in the range of excitation 280–310 nm (35,700–32,250  $\text{cm}^{-1}$ ) and increases significantly by excitation above 310 nm. In the range 310–335 nm the compound demonstrates very broad fluorescence with a maximum of about 450 nm. At 330 nm (30,300  $\text{cm}^{-1}$ ) the emission is very strong and with quantum yields 2–3 times higher than at other excitation wavelengths. By excitation above 340 up to 400 nm (29,400–25,000  $\text{cm}^{-1}$ ) a splitting of signal, with well-separated two fluorescent peaks at 450 nm and 520 nm was observed. Upon excitation above 400 nm the intensity of the first peak decreases rapidly and a

small peak with energy gap of about 2920  $\text{cm}^{-1}$ , in comparison to the excitation wavelength, attended in emission spectra up to 450 nm excitation together with a wide emission peak at 520 nm. Our attention should be directed to the very broad spectral range of fluorescence at 330 nm excitation. Such a spectrum gives potential for the design of white-light emitting materials on the basis of CAID chromophores. White-light emitters on the basis of ESIPT chromophores have been proposed in [9, 32].

We may note that in the emission spectra was observed a very sensible dependence of the intensity of scattered signal on excitation wavelength. This suggests a significant role of resonance light scattering from the investigated compound. For this reason the solutions of CAID in ethanol, PBS and DMSO were investigated in synchronic mode of changing of excitation and emission wavelength on the fluorimeter. On Fig. 6 are shown the observed fluorescence signals when the excitation and emission wavelengths were synchronously changed in the range 200–750 nm with constant differences between them –  $d$ , equal respectively to 0, 5, 10, 25, 50 and 70 nm. The results obtained by  $d = 0$  correspond to the case of resonance light-scattering (RLS). The observed intensity of signal  $I_{OB}$  in such conditions may be presented as a superposition of intensities of fluorescence  $I_F$  and scattering signals  $I_S$  and the level of this signal in case of CAID excitation is several time more than fluorescence intensity value at other conditions.

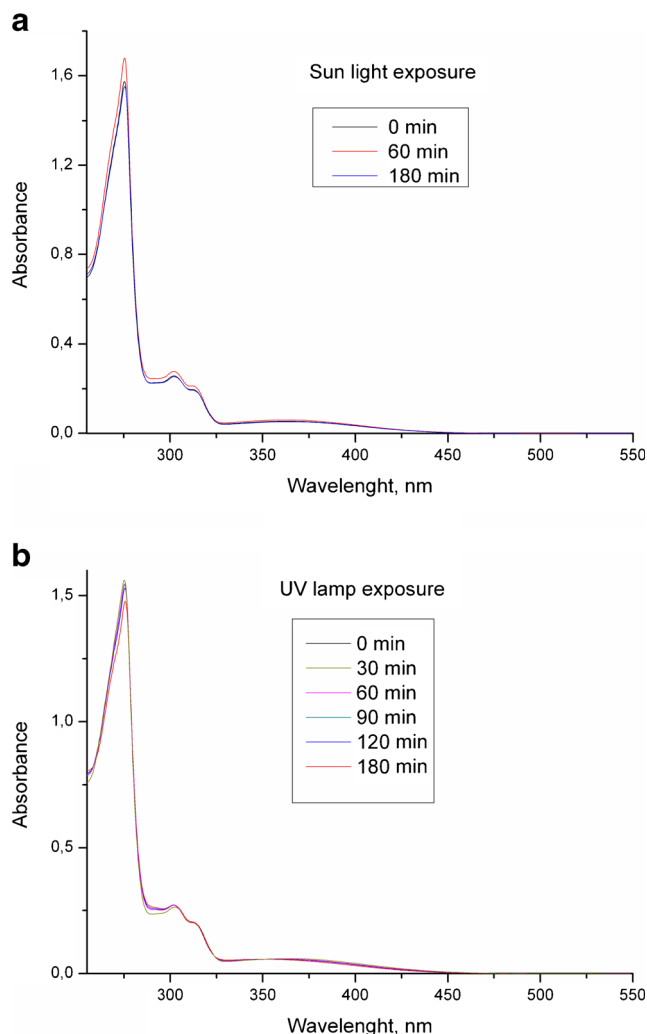


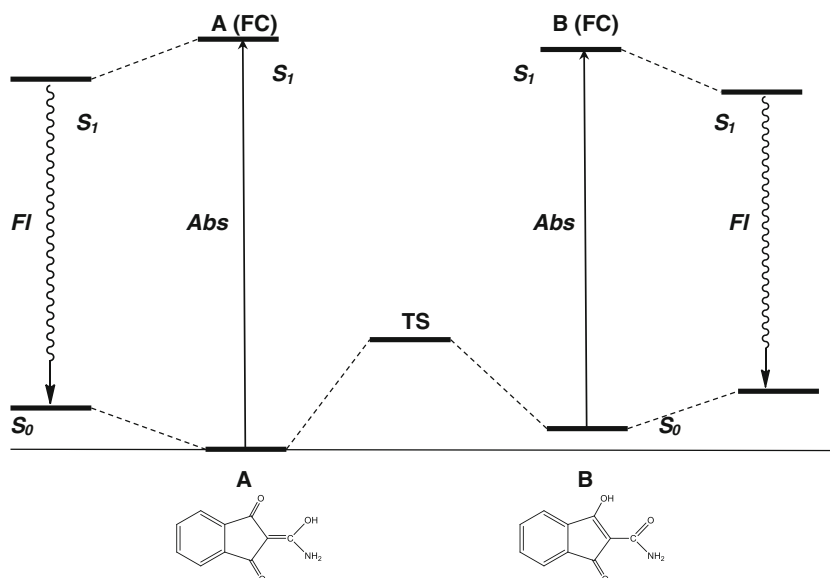
**Fig. 3** UV-vis absorption spectra of CAID in ethanol ( $5 \times 10^{-6}$  M): sunlight exposure (a) and UV lamp exposure (b)

Because of linear dependence of  $I_F$  on absorbance, we assume that  $I_{OB}$  is proportional to the cross section of absorption and scattering [33, 34]. The one of reasons for applying the technique of RLS in compound investigations is that the absorption and scattering cross sections depends on particle size in very different ways. In accordance with [33, 34] for particles with size small compared to the wavelength  $\lambda$ , the absorbance is proportional to  $1/\lambda$  and scattering – to  $V/\lambda$ , where  $V$  is particle volume. Thus, the above consideration leads to the conclusion that larger particles present in the observed signal as a higher scattering and the results obtained at such condition should be useful for particle size dependent experiments, for example where aggregation processes occurs.

As it is shown on Fig. 6 the results obtained under condition for RLS (at  $d = 0$ ) are very different in comparison with fluorescence spectra obtained at  $d \neq 0$  and at fixed excitation (Fig. 5b). The observed fluorescence does not be explained only with the contribution of scattering, because of existing of well-defined peaks at several wavelengths. For explain the results it is necessary of additional experiments, which are not object of this investigation.

For fluorescent probes with application in biological objects, the position of the excitation and emission bands in comparison to those of the investigated objects is very important. For example, for most proteins the intrinsic protein fluorescence originates from the aromatic amino acids (natural fluorophores) tyrosine, tryptophan and phenylalanine with the maximum of excitation bands respectively 275, 295 and 260 nm. The emission maximums are respectively 304, 353 and 282 nm. There is currently interest in the emission from intrinsic fluorophores from tissues and from fluorophores that are also not enzyme cofactors such as nicotinamide adenine

**Fig. 4** Energy diagram of tautomerization for CAID and absorption emission processes





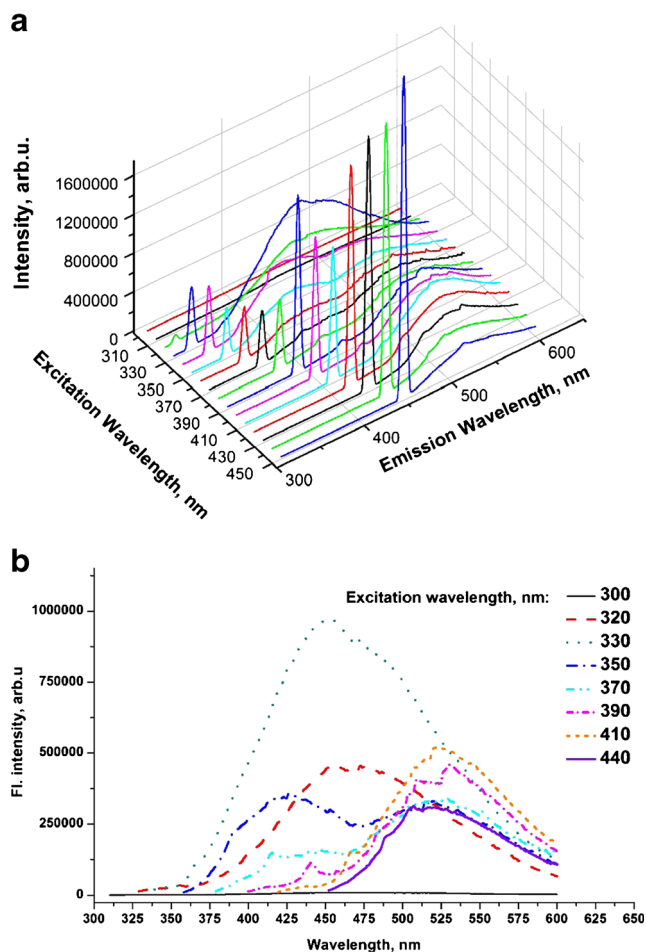


**Fig. 5** 3D excitation-emission spectra of CAID in ethanol (a) and fluorescence at different excitation wavelengths (b)

dinucleotide (NADH) with excitation and emission respectively at 450 and 525 nm [35, 36].

An excitation spectrum for the investigated compound is shown on Fig. 7. The excitation spectra for two emission wavelengths – 450 and 520 nm, corresponding to the obtained maxima on emission spectra, are presented. Both emission wavelengths are of high intensity upon excitation in the range 230–250 nm, and correspond to the transitions  $S_0 \rightarrow S_6$  and  $S_0 \rightarrow S_7$  (Table 2). A very weak emission is observed in the spectrum upon excitation between 280 and 300 nm. For the first emission wavelength in the range 320–400 nm a very broad and intensive excitation band is observed. This band should be fitted with four exponents with  $R^2 = 0.997$  and with peaks at 326, 337, 356 and 382 nm, respectively. Essentially wide, but not so strong excitation band was observed for second fluorescence peak at 520 nm. The fitting procedure gives peaks at 325, 333, 356 and 418 nm with the same  $R^2$  value. Upon comparison of these values with theoretically calculated ones for  $S_0 \rightarrow S_1$ ,  $S_0 \rightarrow S_2$  and  $S_0 \rightarrow S_3$  transitions (Table 2), it is evident that there are significant differences.

The obtained differences suggest that one of the possibilities for such fluorescence behavior should be associated with

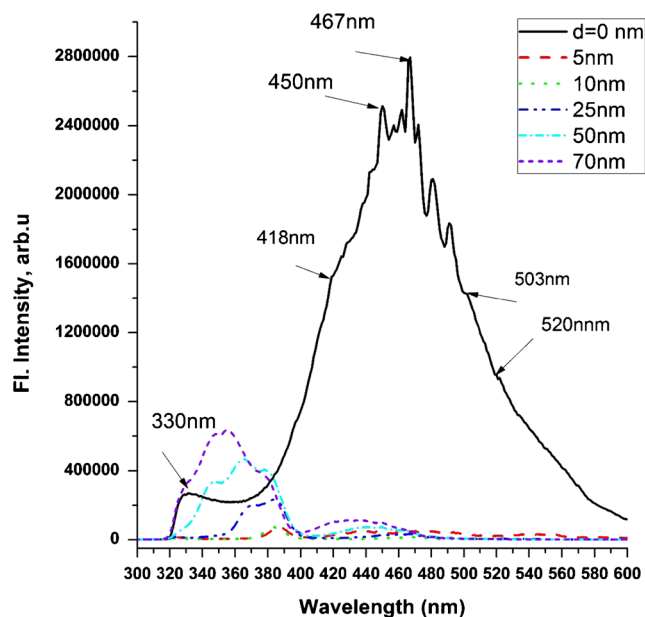


**Fig. 6** Emission spectra in ethanol obtained for CAID by “synchro” experiments with shift between excitation and emission wavelengths respectively 0, 5, 10, 25, 50 and 70 nm

ESIPT. For verification of this assumption the fluorescence lifetime and fluorescence decay behavior at three wavelengths for fluorescence spectra upon excitation with 365 nm and 50 ps long light pulses from a diode laser were investigated. Time resolution of the registration system was evaluated at approximately 82 ps. The fluorescence intensity decay curves at 420, 450 and 520 nm, the wavelengths corresponding to the observed maxima in the fluorescent spectra of CAID are shown on Fig. 8. The decay curves at 420 and 450 nm have bi-exponential character with fast and slow components respectively in the pico- and nanosecond range. The contribution of the shorter lifetime component for both wavelengths according to expression (2) is less than 5 %. The obtained lifetimes are close to each other and eventually every one corresponds to one of the two excited tautomeric forms. The value of the standard deviation of  $\chi^2$  factor (CHISQ) obtained by both fittings procedures in TCSPC measurements is very near to 1, which is one of the conditions for correct determination of fluorescence lifetime values. The presence of two fluorescence lifetimes in the expression for CAID at 420 and 450 nm could be explained with the help of two or three assumptions. The first suggests that such behavior is due to the formation of aggregates which are non-fluorescent, but which can quench the monomer forms [37], resulting in observation of quenched (fast component) and unquenched lifetimes. Because this takes place in a time interval in which excitation is “on” this suggestion for the fast components should be associated also with ESIPT phenomena of enol and keto forms of CAID tautomer because ESIPT process should be more probable in the presence of excitation and therefore fast decay predominantly takes place only in the

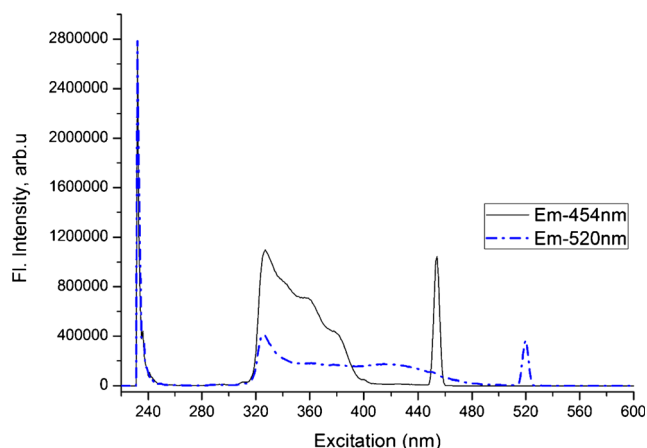


**Fig. 7** Excitation spectra for two different emission wavelengths for CAID

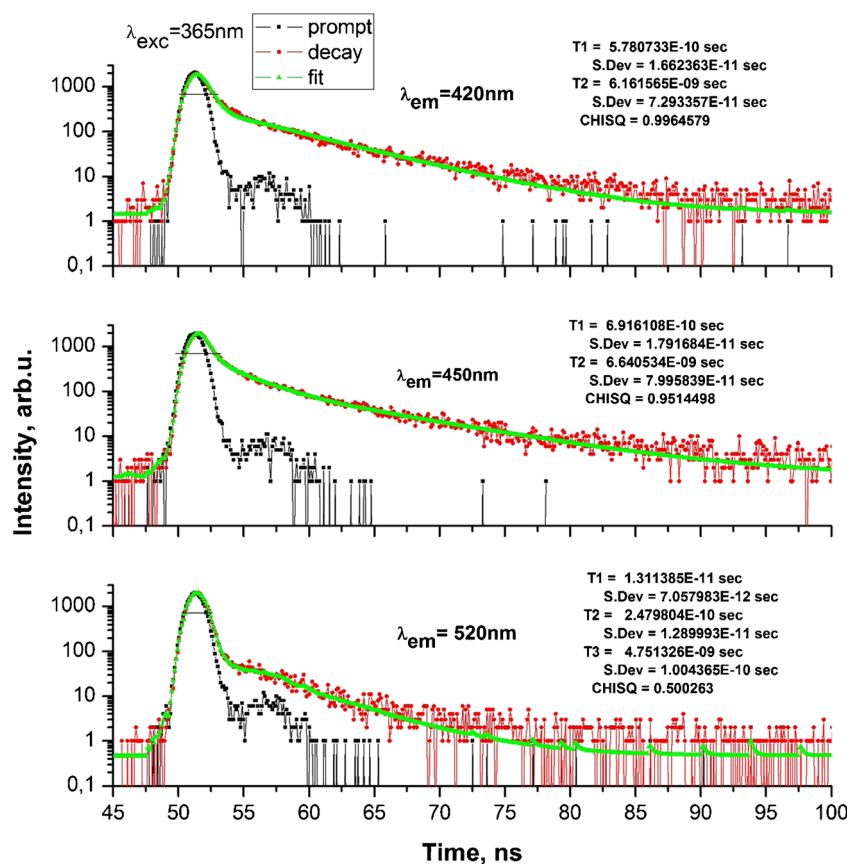
presence of an excitation field which stimulates electrostatic interactions as an origin for aggregation processes.

A different fluorescence decay behavior can be observed at 520 nm. All experiments show that the decay is different from monoexponential. The obtained fluorescence lifetime is by about 2 ns less than the lifetime for others wavelengths. The fitting procedures for bi- and three-exponential decay curves are with results for the CHISQ factor of about 0.5. The lifetime for the fast decay component is about 230 ps and it is two times less than the same component for 420 and 450 nm. The

contribution of the fast decay in the expression of the fluorescence decay curve is about 3.5 %. It may be suggested that in the excited state the two tautomeric forms of CAID are in equilibrium and the quenching process is faster, because it can be associated with ESIPT in two directions – from tautomer A\* to tautomer B\* and reverse. When the fluorescence lifetime decay is fitted with three exponential decay curves, the CHISQ factor is the same, but a very fast component with duration  $13 \pm 7$  ps and contribution of about 0.5 % exists in the expression but this is over the limit for time resolution of the system. Such results may be associated with the time for proton transfer, corresponding to the results obtained in [38] where the measured time for proton transfer for one of conformation form of investigated Schiff base compounds is 10 ps.

Chou et al. [32] proposed that in the case of two exponential decay fluorescence curves described fluorescence life time of a tautomer compound, the faster dynamics component of population changes be assigned to an ESIPT process. The slower decay component of the fluorescence was attributed to the population decay from the excited state through radiative and non-radiative processes. If we assume such a suggestion, because of significant differences in faster dynamics parts of fluorescence decay of 240, 570 and 700 ps corresponding to the transitions at 520, 420 and 450 nm respectively it can be concluded that there are

**Fig. 8** Fluorescence decay curves for three different wavelengths and excitation at 365 nm

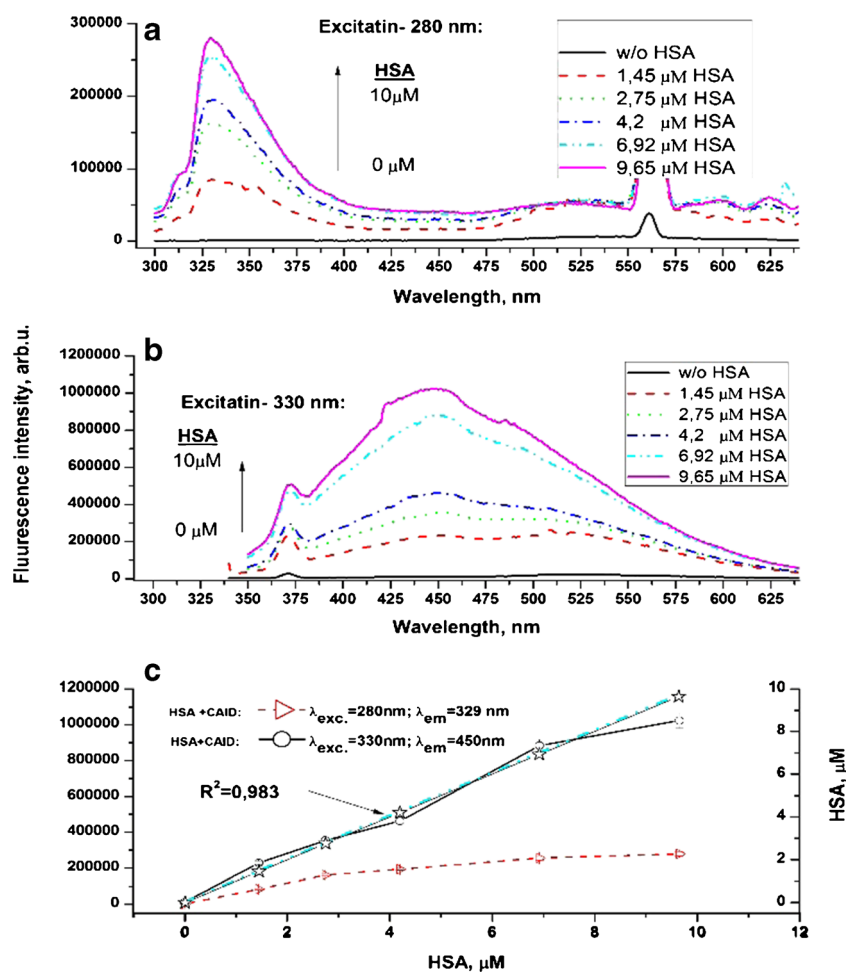


two different ways for proton transfer for the excited state of CAID. The first one is from A\* to B\* tautomeric form and the second way probably should be associated with proton transfer from the amino group to the oxygen atom on the indanedione moiety. For a more detailed explanation how the observed curves are associated to the energy diagram for tautomeric form of CAID (Fig. 4, Table 2) it is necessary to obtain the time dependence for transient absorption related to the above fluorescence wavelengths. The suggestion that at this excitation it is possible to observe transient behavior of excited state population and respectively fluorescence decay curves is confirmed also from the delay of fluorescence intensity maximum to the maximum of excitation. For 520 nm it is about 100 ps, for 420 nm delay it is 150 ps and for 450 nm – about 200 ps.

The fluorescent properties of conjugation between CAID and HSA and CAID with DNA sequences were studied for evaluation of the possibility for applying of CAID as a fluorescent probe in biological investigations. The CAID fluorescence behavior at constant concentration of the compound as a function of excitation wavelength and concentration of HSA is shown on Fig. 9. The observed fluorescence from 25  $\mu\text{M}$  of

CAID in saline phosphate buffer (pH = 7.4) at room temperature is very weak upon excitation at 330 nm or near zero upon excitation at 280 nm because of poor solubility in water. The measurements of protein and CAID binding properties were made after adding consecutively in solution a small quantity of HSA and keeping mixture for 5 min before running of the fluorescent spectra. The obtained spectra are shown on Fig. 9a,b. The excitation wavelengths 280 nm and 330 nm were chosen with regards to maxima of absorption of HSA and CAID, respectively. Upon excitation with 280 nm in the present fluorescent spectra, intensive HSA fluorescence with a maximum at 330 nm was observed. The intensity of this fluorescence increases with increasing concentration of HSA. A very wide fluorescence associated with CAID was observed. It may be remarked that around 520 nm the fluorescence intensity is not be influenced by the concentration of added HSA, while at all spectral range such an influence was observed. Two local peaks at 595 nm and at 620 nm (shown on Fig. 9a) which are not observed in normal fluorescence spectra of CAID (Fig. 5a,b) can be detected. The second one should be associated with the theoretical predicted fluorescence of tautomer B. The fluorescence of CAID at 280 nm

**Fig. 9** The fluorescence intensity of CAID depending on concentration of HSA at two excitation wavelengths: 280 nm (a), 330 nm (b) and determining of HSA concentration (c) with the help of CAID-HSA mixture fluorescence (\* -real HSA concentration)



excitation could be explained with Förster resonance energy transfer (FRET) because of overlapping of emission spectra of HSA with absorption spectra of CAID. As reported in [39] in the case of labeling of bovine serum albumin (BSA) with benzoazoles, which relax by an ESIPT mechanism, the authors refer to the fact, that there are many residues in BSA which may be available as potential sites for binding. In our case, after adding of HSA in solution, concerning the observed fluorescence it may be proposed that CAID effectively binds to such sites. The strong emission from HSA at 330 nm in result of absorbed from HSA excitation at 280 nm, effectively excite the CAID probe through both mechanisms: (i) absorption of emitted light from non-bound CAID molecules and (ii) FRET for bound molecules. The fluorescence spectra obtained by titration of constant concentration of HSA with different concentrations of CAID (not shown) demonstrated that investigated compound significantly quenched HSA fluorescence at 330 nm. The nonlinear character of dependence of fluorescence intensities of CAID and HSA on HSA concentration (Fig. 9c, curve for emission at 330 nm) clear demonstrate the limitation for use as molecular probes of fluorescent compounds in which the excitation is achieved through the FRET mechanism. As a result of several photophysical processes which take place in various interactions of photons with the investigated matter, the nonlinearities at higher concentration are intrinsic according to the observed results.

When the solutions with different concentration of HSA were excited at 330 nm (Fig. 9b), the fluorescent spectra showed that there is direct excitation of the CAID molecules. This is also confirmed from the linear dependence of CAID fluorescence intensity on HSA concentration (Fig. 9c, curve for emission at 450 nm). Probably this means that in case of HSA labeling with CAID molecules there is one binding site for interaction of HSA with CAID. This behavior gives possibilities to use CAID as probe for determination of concentration of such proteins and the wide absorption spectra of CAID permit to find an excitation spectra range in which FRET should be disappearing.

The possibility of CAID to bind to DNA sequences (DNAs) is demonstrated on the basis of the fluorescence measurements (Fig. 10). In this case 12-mer double stranded DNA (dsDNA) labeled with fluorescent dye carboxytetramethylrhodamine (TAMRA) at 5-position (Fig. 10a) was used as target for verification capabilities for DNA labeling with CAID. In TRIS (trishydroxymethyl aminomethane) based buffer, first were added CAID to obtain concentration 10  $\mu$ M and after 5 min the two different fluorescent spectra were recorded – first at several fixed excitation wavelengths and second using “synchro” excitation technique with zero difference between excitation and emission wavelengths. After adding to the solution of the DNA sequences, labeled with TAMRA (one of many rhodamine derivatives used for labeling purposes) and keeping the above procedure, the fluorescence spectra for CAID at

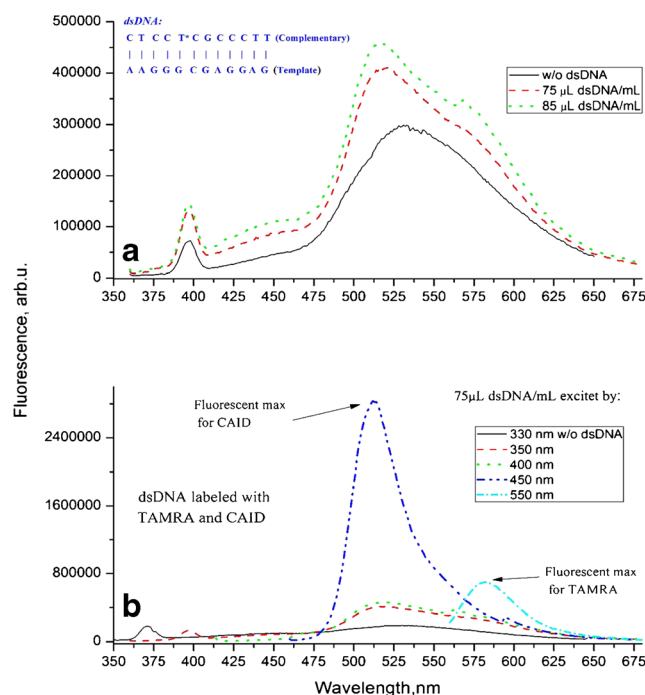


**Fig. 10** Emission spectra for DNA sequences labeled with CAID and rhodamine at different excitation wavelengths

different concentration of DNAs were registered. In case of “synchro” experiments, the spectra are the same as those shown on Fig. 6 for  $d = 0$ , and they are sensitive to the DNAs concentration. The shape of the fluorescence curve is smoother when DNAs and CAID are present in solution in comparison with fluorescence curve for solution only with CAID. The sensitivity of labeling of DNA sequences with CAID to the concentration of DNAs is demonstrated on Fig. 10a upon excitation at 330 nm. The obtained results indicate that small changes in the concentration of DNA can be detected. In the same time it was observed significant shift (16–17 nm) of fluorescence maxima of CAID to the shorter wavelengths in the presence of DNA. The shift value is independent of DNA concentration and this may be explained with eventual forming of hydrogen bond between CAID and DNA parts.

The ratios between fluorescent signals from both fluorescent probes – TAMRA and CAID upon excitation at different wavelengths are shown on Fig. 10b. Only upon excitation with wavelengths longer than 525 nm the fluorescence signal from TAMRA probe presence in spectra and it is higher than that one from CAID. On the basis of these results for concentration and excitation wavelength dependence observed at CAID-DNA fluorescent spectra and chemical structure of CAID could be proposed as molecular probe for DNA sequences alone or in combination with another molecular probe.

The photostability properties of fluorescent probes are very important for fluorescence spectroscopic investigation. From this point of view the photostability properties of CAID as a



solution in ethanol ( $5 \times 10^{-6}$  M) was studied by following the absorbance during natural light irradiation at noon of a hot summer day (July, 21st, 2011) (Fig. 3a). The recorded absorption spectra suggested relatively high photostability within 3 h irradiation period. In case of sun light the strongest peak at 275 nm decreases after the first hour by 9 % and stays stable until the end of the irradiation time.

The photostability behavior of CAID in ethanol solution slightly differs during UV lamp irradiation (Fig. 3b). The band with a maximum at 375 nm has approximately the same intensity and drops negligible after 3 h UV irradiation. During the two irradiation conditions (sun light and UV lamp) the broad shaped wavelength at 375 nm appears stable showing one of the same absorption intensities. Therefore, on the basis of the observed insignificant photobleaching effect of the CAID molecule upon irradiation and the fact that excess energy is dissipated by emission of higher wavelengths without photochemical decomposition of the molecule. Such behavior of the investigated compound supposes possibilities for using of the CAID molecule also as photoprotector of human skin because of strong absorption in UVA, UVB and UVC light spectra and dominantly dissipating of absorbed energy subsequently by non-radiation transitions or by radiation in visible spectrum above 420 nm.

## Conclusion

The chemical structure of 2-carbamido-1,3-indandione suppose that CAID could be act as a proton donor in hydrogen bonding interactions. Such possibility, the suitable spectral ranges of absorption and fluorescence, and the high fluorescence quantum yield are advantages of this compound for probing biomolecules of high importance for biology and medicine, as well as for use in sunscreens.

**Acknowledgments** The authors are grateful to Dr. Ekaterina Borisova and Ms. Alexandra Zhelyazkova, Institute of Electronics, Bulgarian Academy of Sciences for technical support. Two of the authors (IA and VM) acknowledge the financial support of the National Science Fund under grant DFNI-02/9/2014.

## References

- Horton RL, Murdock KC (1960) 2-substituted 1,3-indandiones. *J Org Chem* 25:938–941
- Enchev V, Abrahams I, Angelova S, Ivanova G (2005) Fast intramolecular proton transfer in 2-(hydroxyaminomethylidene)-indan-1,3-dione. *J Mol Struct Theochem* 719:169–175
- Angelova S, Enchev V, Kostova K, Rogojerov M, Ivanova G (2007) Theoretical and spectroscopic study of 2-substituted indan-1,3-diones: a coherent picture of the tautomeric equilibrium. *J Phys Chem A* 111:9901–9913
- Song J, Mishima M, Rappoport Z (2007) Isomeric solid enols on ring- and amide-carbonyls of substituted 2-carbanilido-1,3-indandiones. *Org Lett* 9:4307–4310
- Lakowicz JR (2006) *Principles of Fluorescence Spectroscopy*. Springer, Third Edition
- Demchenko AP (2014) Practical aspects of wavelength ratiometry in the studies of intermolecular interactions. *J Mol Struct* 1077: 51–67
- Wu J, Liu W, Ge J, Zhang H, Wang P (2011) New sensing mechanisms for design of fluorescent chemosensors emerging in recent years. *Chem Soc Rev* 40:3483–3495
- Craig IM, Duong HM, Wudl F, Schwartz BJ (2009) A new route to dual fluorescence: spectroscopic properties of the valence tautomers of a 3-(2H)-isoquinolinone derivative. *Chem Phys Lett* 477: 319–324
- Zhao J, Ji S, Chen Y, Guo H, Yang P (2012) Excited state intramolecular proton transfer (ESIPT): from principal photophysics to the development of new chromophores and applications in fluorescent molecular probes and luminescent materials. *Phys Chem Chem Phys* 14:8803–8817
- Demchenko AP (2006) Visualization and sensing of intermolecular interactions with two-color fluorescent probes. *FEBS Lett* 580: 2951–2957
- Galindo F, Becerril J, Isabel Burguete M, Luis SV, Vigara L (2004) Synthesis and study of a cyclophane displaying dual fluorescence emission: a novel ratiometric sensor for carboxylic acids in organic medium. *Tetrahedron Lett* 45:1659–1662
- Ercelen S, Klymchenko AS, Demchenko AP (2003) Novel two-color fluorescence probe with extreme specificity to bovine serum albumin. *FEBS Lett* 538:25–28
- Goswami S, Maity S, Das AK, Maity AC, Mandal TK, Samanta S (2013) Remarkable ESIPT induced NIR emission by a selective colorimetric dibenzimidazolo diimine sensor for acetate. *Tetrahedron Lett* 54:5232–5235
- Suh D, Chaires JB (1995) Criteria for the mode of binding of DNA binding agents. *Bioorg Med Chem* 3:723–728
- Rai R, Srinivas CR (2007) Photoprotection. *Indian J Dermatol Venereol Leprol* 73:73–79
- Bruls WA, Slaper H, van der Leun JC, et al. (1984) Transmission of human epidermis and stratum corneum as a function of thickness in the ultraviolet and visible wavelengths. *Photochem Photobiol* 40: 485–494
- Cadet J, Sage E, Douki T (2005) Ultraviolet radiation-mediated damage to cellular DNA. *Mutat Res* 571:3–17
- De Fabo EC, Noonan FP (1983) Mechanism of immune suppression by ultraviolet irradiation in vivo. I evidence for the existence of a unique photoreceptor in skin and its role in photoimmunology. *J Exp Med* 158:84–98
- Heck DE, Vetrano AM, Mariano TM, et al. (2003) UVB light stimulates production of reactive oxygen species: unexpected role for catalase. *J Biol Chem* 278:22432–22436
- Gonzalez S, Gilaberte Y, Philips N, Juaranz A (2011) Current trends in photoprotection - a new generation of oral photoprotectors. *Open Dermatol J* 5:6–14
- Gonzalez C, Schlegel HB (1989) An improved algorithm for reaction path following. *J Chem Phys* 90:2154–2161
- Cossi M, Rega N, Scalmani G, Barone V (2003) Energies, structures, and electronic properties of molecules in solution with the C-PCM solvation model. *J Comput Chem* 24:669–681
- Bauerschmitt R, Ahlrichs R (1996) Treatment of electronic excitations within the adiabatic approximation of time dependent density functional theory. *Chem Phys Lett* 256:454–464
- Dreuw A, Head-Gordon M (2005) Single-reference ab initio methods for the calculation of excited states of large molecules. *Chem Rev* 105:4009–4037



25. Becke AD (1993) Density-functional thermochemistry. III The role of exact exchange. *J Chem Phys* 98:5648–5652
26. Lee C, Yang W, Parr RG (1988) Development of the colle-salvetti correlation-energy formula into a functional of the electron density. *Phys Rev B* 37:785–789
27. Hariharan PC, Pople JA (1973) The influence of polarization functions on molecular orbital hydrogenation energies. *Theor Chim Acta* 28:213–222
28. Francel MM, Pietro WJ, Hehre WJ, Binkley JS, Gordon MS, Defrees DJ, Pople JA (1982) Self-consistent molecular orbital methods. 23. A polarization-type basis set for 2nd-row elements. *J Chem Phys* 77:3654–3665
29. Schmidt MW, Baldridge KK, Boatz JA, Elbert ST, Gordon MS, Jensen JH, Koseki S, Matsunaga N, Nguyen KA, Su S, Windus TL, Dupuis M, Montgomery JA (1993) General atomic and molecular electronic structure system. *J Comput Chem* 14:1347–1363
30. Gordon MS, Schmidt MW (2005) Advances in electronic structure theory: GAMESS a decade later. In: Dykstra CE, Frenking G, Kim KS, Scuseria GE (eds) *Theory and applications of computational chemistry: the first forty years*. Elsevier, Amsterdam, pp. 1167–1189
31. Magde D, Wong R, Seybold PG (2002) Fluorescence quantum yields and their relation to lifetimes of rhodamine 6G and fluorescein in nine solvents: improved absolute standards for quantum yields. *Photochem Photobiol* 75:327–334
32. Tang K-C, Chang M-J, Lin T-Y, Pan H-A, Fang T-C, Chen K-Y, Hung W-Y, Hsu Y-H, Chou P-T (2011) Fine tuning the energetics of excited-state intramolecular proton transfer (ESIPT): white light generation in a single ESIPT system. *J Am Chem Soc* 133: 17738–17745
33. Bohren CF, Huffman DR (1983) *Absorption and scattering of light by small particles*. John Wiley and Son Inc., New York
34. Pasternack RF, Bustamante C, Collings PJ, Giannetto A., Gibbs EJ (1993) Porphyrin assemblies on DNA as studied by a resonance light-scattering technique. *J Am Chem Soc* 115: 5393–5399.
35. Palmer GM, Keely PJ, Breslin TM, Ramanujam N (2003) Autofluorescence spectroscopy of normal and malignant human breast cell lines. *Photochem Photobiol* 78:462–469
36. Da Costa RS, Andersson H, Wilson BC (2003) Molecular fluorescence excitation-emission matrices relevant to tissue spectroscopy. *Photochem Photobiol* 78:384–392
37. Lacey JA, Phillip D (2002) Fluorescence lifetime measurements of disulfonated aluminium phthalocyanine in the presence of microbial cells. *Photochem Photobiol Sci* 1:378–383
38. Ziolek M, Kubicki J, Maciejewski A, Naskrecki R, Luniewski W, Grabowska A (2006) Unusual conformational effects in proton transfer kinetics of an excited photochromic Schiff base. *J Photochem Photobiol A* 180:101–108
39. Rodembusch FS, Leusin FP, da Costa Medina LF, Brandelli A, Stefani V (2005) Synthesis and spectroscopic characterization of new ESIPT fluorescent protein probes. *Photochem Photobiol Sci* 4:254–259